TASK QUARTERLY 5 No 4 (2001), 537–547

A CFD PACKAGE FOR THE 3D NAVIER-STOKES COMPUTATION OF UNSTEADY FLOWS IN TURBOMACHINES

HANS THERMANN, STEPHAN SCHMIDT,
CARSTEN WEIß AND REINHARD NIEHUIS

Institut für Strahlantriebe und Turboarbeitsmaschinen, RWTH Aachen,
Templergraben 55, 52062 Aachen, Germany
thermann@ist.rwth-aachen.de
http://www.ist.rwth-aachen.de

(Received 31 July 2001; revised manuscript received 15 August 2001)

Abstract: A 3D Navier-Stokes package for the time-accurate computation of unsteady flows in turbomachines with emphasis on wide applicability, portability and efficiency is presented. The package consists of three components: the elliptic grid generator FRAME, the parallelised implicit Reynolds- and Favre-averaged Navier-Stokes solver PANTA and the post-processor TREAT especially designed for unsteady flow phenomena. The applicability of the package covers both rotor/stator interaction and blade flutter phenomena in multirow and multipassage 2D, Quasi3D and general 3D configurations in a wide range of flow velocities (subsonic, transonic). For turbulent computations either a Low-Reynolds-Number k-ε or k-ω turbulence model is available. Additionally, an algebraic transition model can be chosen from a variety of different models to enhance the accuracy of prediction for transitional flow phenomena. A description of the underlying algorithms and numerical methods as well as the main features and characteristics of each of the three components is given. Furthermore, selected examples of typical turbomachinery applications are shown to demonstrate these features.

Keywords: CFD, turbomachinery, laminar-to-turbulent transition, flutter, clocking

1. Introduction

Computational fluid dynamics have become an important tool in the design process of modern turbomachines. With their help, costly experimental investigations can be avoided and development times can be shortened. Furthermore, CFD allows detailed investigations of certain flow phenomena early in the design phase, which may lead to a better understanding of the flow physics in turbomachines.

A time-accurate, three-dimensional CFD package for the computation of viscous, unsteady flows in turbomachines has been developed at the Institute for Jet Propulsion and Turbomachinery of the RWTH Aachen by Benetschik *et al.* [1] and Brouillet *et al.* [2]. The

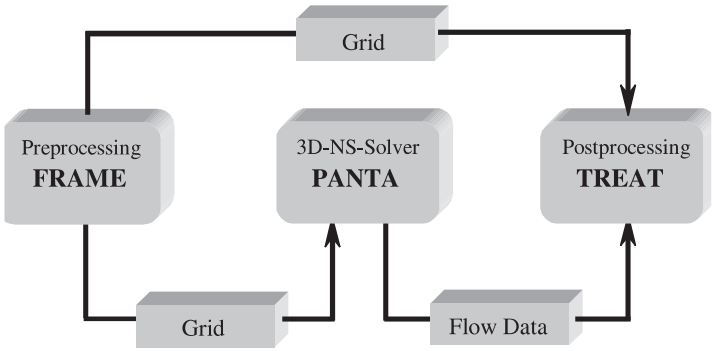

Figure 1. CFD package

package, which is presented in this paper, consists of the three-dimensional, elliptic grid generator FRAME, the Navier-Stokes flow solver PANTA and the post-processor TREAT.

2. The grid generator frame

An important issue in computational fluid dynamics is the generation of grids. While grids have to be fine enough to resolve the physical phenomena, a smaller number of points is desired to allow fast computations. Consequently, grids are refined in areas where characteristic scales are small, such as in boundary layers or in highly disturbed flows, and are held coarse anywhere else in the computational domain. Furthermore, a maximum orthogonality and smoothness of the grid is required to avoid numerical diffusion.

A prerequisite for grid generation is an exact definition of the geometry. In the grid generator FRAME the geometry has to be defined in discrete Cartesian coordinates. The geometry of hub and casing is transformed into a meridian coordinate m and an angle θ. The meridian coordinate m enables a one-valued function for radial as well as axial machines. The meridian layers are then staggered between hub and casing using a one-dimensional distribution based either on an algebraic algorithm or an elliptic equation. For the profile a bicubic surface spline is applied and the intersections with the meridian layers are computed. Since the splines are defined by nonlinear functions a Newton iteration has to be performed to find the intersections.

Grid generation techniques can be divided into two basic categories: algebraic methods, which are based on the interpolation of points, and methods solving partial differential equations (Thompson [3]). The grid generator FRAME is based on the elliptic Poisson equations:

$$\nabla^2 \xi_i = Q_i \quad i = 1,2 \tag{1}$$

The source terms Q_i on the right hand side are used to control the grid refinements. An advantage of elliptic techniques is that the requirements of smoothness and exclusion of overlapping can be met. The source terms are defined as proposed by Sorenson [4]. Since four local source terms need to be specified, two conditions at each boundary can be enforced to control the grid refinements. These conditions are the width of the first cell and the angle of the first grid line relative to the boundary (typically 90°). The refinements within the computational domain can be controlled by exponential parameters. For the purpose of general applicability a user friendly interface has been implemented. Optimal

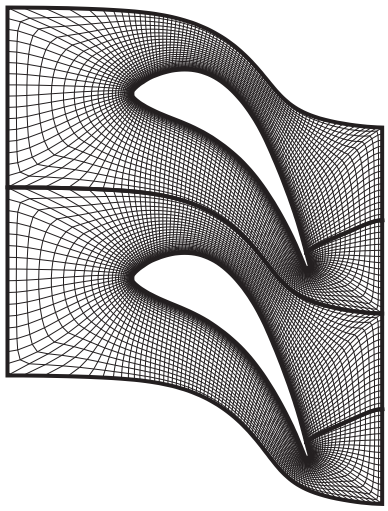

Figure 2. Grid at midspan of an axial turbine

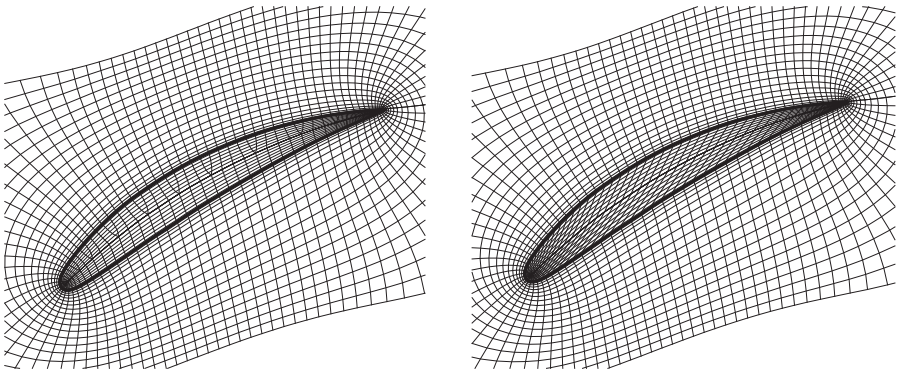

Figure 3. Clearance grid with (left) and without (right) double points along the centerline

values are automatically assigned to missing parameters. Thus, grid generation turnaround times are minimised.

2.1. Examples

FRAME can handle both plane and cylindrical configurations. Either two- or three-dimensional grids may be generated. The program is structured into separate modules that can be combined individually for specific applications. The basic algorithm computes a single C-, O- or H-type grid with one profile. Besides, a splitter, a clearance grid, an in- and outflow block or an O-type mesh in the boundary layer region can easily be added. To gain maximum orthogonality, a shift of points at the outer boundary can be conducted. Further contributions to orthogonality in the case of high turning blades can be achieved by a free positioning of the cut line (Figure 2). Additionally, a solution of the elliptic equations across the periodic boundaries yields a smooth grid at the outer boarders. Since this leads to a different number of points on the suction and pressure sides of the blade, the deformation of the clearance grid can be avoided by adding double points along the centerline (Figure 3).

3. The post-processor TREAT

The post-processor TREAT realises an interface between the grid generator FRAME, the Navier-Stokes solver PANTA and a commercial visualisation tool. Its main purpose is the transformation of the conservative flow properties into any desired flow quantities. Furthermore, TREAT allows an analysis of periodic unsteady flow phenomena, such as the harmonic analysis of flutter computations.

One important feature of TREAT is the reduction or extension of flow data. On the one hand, the large amount of data obtained from unsteady computations can easily be reduced to the desired, necessary information. On the other hand, TREAT is able to extend the flow data computed for one flow channel onto the whole annulus. Figure 4 shows the instantaneous blade surface pressure for a traveling wave mode flutter computation of a transonic compressor. The computation has been conducted on a single flow channel and the results have been extended onto the whole annulus.

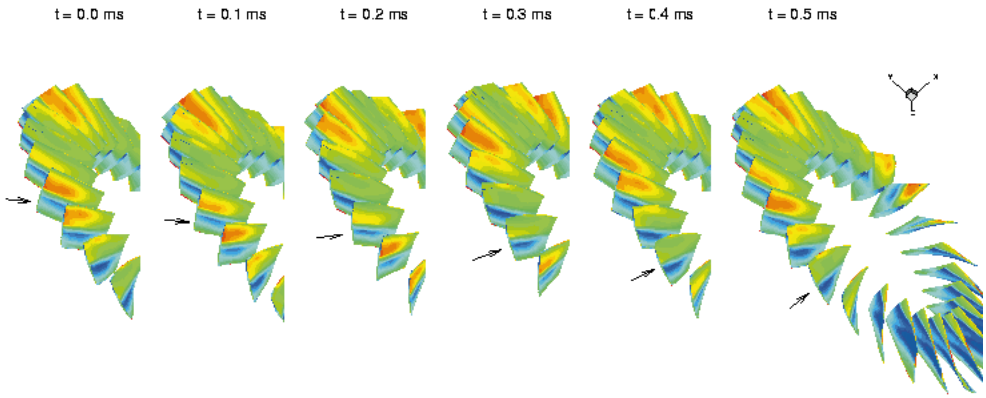

Figure 4. Extension of the plot domain

4. The flow solver PANTA

The three-dimensional, viscous, unsteady flow solver PANTA is based on the compressible Reynolds- and Favre-averaged Navier-Stokes equations using either a Low-Reynolds-Number k-ε or k-ω turbulence model (Chien [5], Biswas and Fukuyama [6], Wilcox [7]). In the three-dimensional case one obtains a system of seven coupled differential equations:

$$\frac{\partial \vec{Q}}{\partial t} + \frac{\partial \vec{F}_i}{\partial x_i} = \frac{\partial \vec{F}_{vis,i}}{\partial x_i} + \vec{H}. \tag{2}$$

The vectors $\vec{H}$, $\vec{F}_i$, and $\vec{F}_{vis,i}$ contain the source terms, convective and pressure terms and viscous fluxes, respectively. The vector $\vec{Q}$ contains the conservative state variables:

$$\vec{Q} = (\rho,\ \rho u,\ \rho v,\ \rho w,\ \rho e,\ \rho k,\ \rho\varepsilon\ (\text{or}\ \rho\omega))^T. \tag{3}$$

For transitional flow computations, algebraic transition models are applied, which are based on the intermittency concept originally proposed by Emmons [8]. He defined an intermittency function γ as the probability of a flow being turbulent at a given position. γ varies between 0 for laminar flow and 1 for fully turbulent flow. The intermittency

function γ is computed by transition models that correlate it to characteristic flow properties. It is used to modify the turbulent viscosity yielding:

$$\mu_t^\star = \gamma \cdot \mu_t \tag{4}$$

A cell-centered finite-volume method is used for the spatial discretisation of the conservation equations. The first order spatial deviations are then the differences of the fluxes entering and exiting one cell.

The inviscid fluxes are calculated with the upwind flux-difference splitting method of Roe [9]. The MUSCL-technique of van Leer [10] is applied to achieve an accuracy of second or third order in determining the left and right hand side state vectors. In regions with large gradients the order is limited by a TVD-limiter to avoid numerical instabilities. The interpolation technique of Chakravarthy [11] is applied to calculate the viscous fluxes. The source terms are discretised by central differences.

An implicit method is used for time integration. Since for an implicit scheme the state vector is unknown for the new time step, the non-linear system is solved by Newton iterations. For steady computations only one iteration per time step is needed. For each Newton step the system of equations is solved by a block-Jacobi iterative algorithm.

Computations with PANTA can be performed two-dimensional, quasi-three-dimensional or three-dimensional, steady or unsteady, viscous or inviscid. Furthermore, depending on the configuration, specific modules can be applied such as different turbulence and transition models, a module for rotor/stator interaction or a module for flutter computations. In the following, computational results for selected applications are presented.

5. Application examples

5.1. *Effects of transition modeling*

Müller *et al.* [12] and Thermann *et al.* [13] investigated models which simulate boundary layer transition in turbomachinery flows and showed that computational results may be improved by using additional, algebraic transition models. Computations with the flow solver PANTA using different algebraic transition models were performed for an annular subsonic compressor cascade. The cascade has been experimentally studied by Schulz [14] at the Institute for Jet Propulsion and Turbomachinery.

Figures 5a and 6a show oil flow visualisations of the boundary layers on the pressure and suction side of the blades at an operating point with an inflow yaw angle of $\alpha = 40°$. On the pressure side the flow is almost two-dimensional with a laminar separation bubble (LSB) near the leading edge. On the suction side two turbulent separations at the hub (TS-H) and the casing (TS-C) can be found. At midspan a separated laminar flow region can be identified.

The computations were conducted on a structured O-type mesh with $201 \times 41 \times 41$ nodes with a y^+ of the first cell of about 1. Three different computational methods were applied: fully turbulent, transitional with models for separated-flow transition and transitional with a combination of models for separated and attached flow.

Figures 5 and 6 show a comparison of the computed dimensionless shear stresses c_f on the pressure and suction side with pictures of oil flow visualisations.

In the turbulent solution (Figures 5b and 6b) the turbulent boundary layer is stable enough to resist the adverse pressure gradient and there is no laminar separation bubble

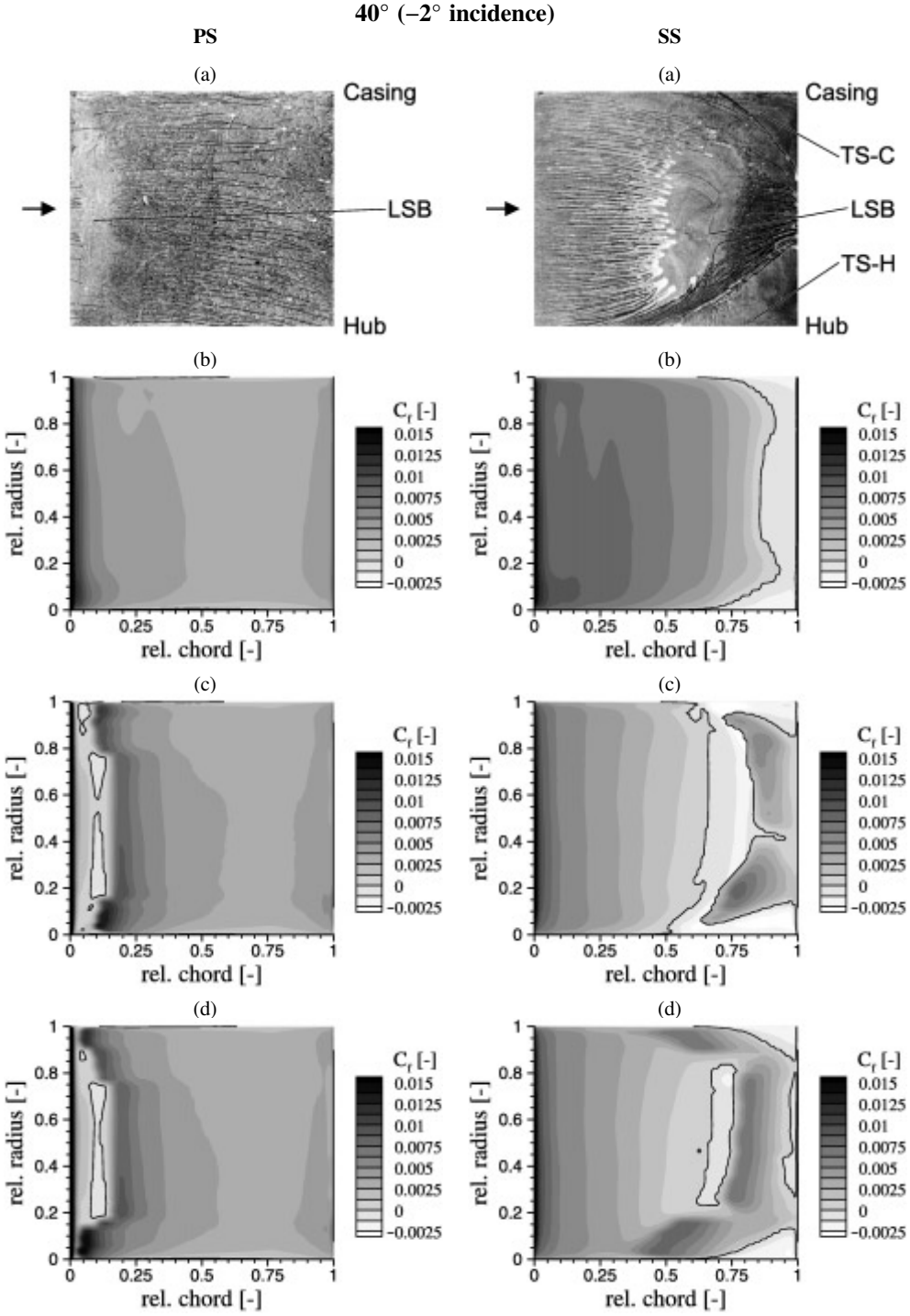

Figure 5. Oil flow visualisation (a) and c_f-distributions on the pressure side ($\alpha = 40°$): (b) turbulent; (c) separated transition; (d) combined transition

Figure 6. Oil flow visualisation (a) and c_f-distributions on the suction side ($\alpha = 40°$): (b) turbulent; (c) separated transition; (d) combined transition

neither on the pressure side nor on the suction side. The computation predicts the turbulent separations at the hub and casing on the suction side but especially the separation at the hub is too small compared to the experiment. The underprediction of the separated regions at the hub and casing may be caused by an overproduction of turbulent kinetic energy near the walls and can be attributed to deficits of the turbulence model (Thermann *et al*. [13]). In contrast to the experiments, a turbulent separation is computed at the trailing edge at the midspan which extends to the hub and casing.

The prediction of the boundary layer development can be improved substantially compared to the fully turbulent solution when applying additional transition models. Figures 5c and 6c show pictures of the skin friction coefficient for computations conducted with the transition criterion of Mayle [15] and the transition model of Walker *et al*. [16] for separated-flow transition. As can be seen, laminar separation bubbles are computed on the pressure and suction side. In contrast to the experiments, the separation bubble extends to the hub and casing on the suction side. On the pressure side several regions of separated laminar flow can be found expanding over the whole blade span.

Since turbulence levels are relatively high near the sidewalls, a bypass transition occurs early in this region. Thus, a later separation of the turbulent boundary layer is suppressed. This effect is neglected in the calculation with models for separated-flow transition. Consequently the laminar separation bubbles extend to the hub and casing.

In order to account for the different transition modes, transition criteria and models for separated and for attached flow are combined. In regions with high turbulence levels, where the location of transition onset is mainly a function of the turbulence level, models for attached flow are applied. In this study the criterion of Sieger *et al*. [17] and the model of Solomon *et al*. [18] for attached flow were combined with the criterion of Mayle [15] and the model of Walker *et al*. [16] for separated flow.

Plots of the shear stress coefficient for computations performed with the combined transition method are shown in Figures 5d and 6d. The laminar separation bubbles on suction and pressure side no longer extend to the sidewalls due to the different transition modes used. The spanwise expansion of the separation bubble is too small compared to the experiment. Since the computation overestimates the turbulence levels near the sidewalls, the regions of attached transition expand too far towards the midspan. Nevertheless, the overall agreement of the measured and computed boundary layer development could further be improved with the use of the presented combined method.

5.2. Stall flutter computations

Flutter computations can be performed with PANTA as Traveling Wave Mode (TWM) computations, conducted on a single blade channel with all blades oscillating with a specified inter blade phase angle, or as Influence Mode (IM) computations, conducted on three or more blade channels with only the center blade oscillating.

Three-dimensional influence mode stall flutter computations of a linear transonic compressor cascade were performed with PANTA by Brouillet *et al*. [2]. The cascade, which was experimentally investigated by Poensgen and Gallus [19] and Ellenberger and Gallus [20] at the Institute for Jet Propulsion and Turbomachinery, consists of nine blades with the center blade being forced to torsional oscillations with a frequency of 310 Hz and an amplitude of 1°. Investigations have been conducted for different Mach-numbers and incidence angles.

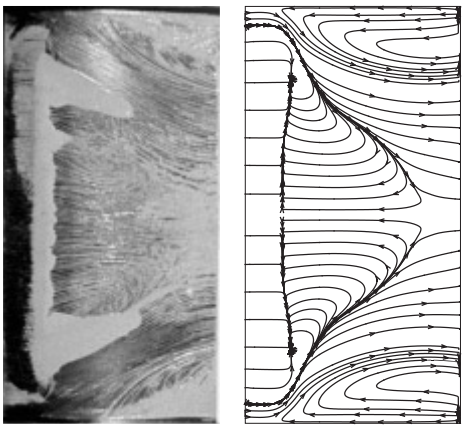

Figure 7. Oil flow visualisation (left) and computed streamlines (right) on the suction side (steady flow)

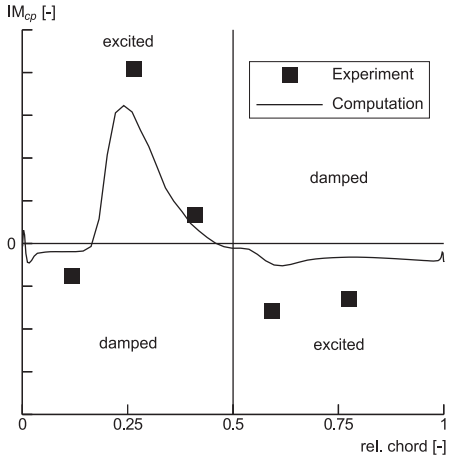

Figure 8. Imaginary part of the dimensionless pressure fluctuations on the suction side of the moving blade

Figure 7, on the left hand side, shows an oil flow visualisation of the steady flow on the suction side of the blade for an operating point with an inflow Mach-number of 0.88 and an incidence of 4°. There is a large separation on the suction side and at the suction-sided endwalls. Furthermore, the flow exhibits a shock at about 25% chord length on the suction side.

On the right hand side of Figure 7, streamlines of a steady transitional computation are shown. Here, a specified transition field was used, since the algebraic transition models were not available at the time of computations. As can be seen, the computed midspan separation as well as the side wall separations agree well with the experiment.

Unsteady computations were performed for five blade channels with the center blade oscillating. One significant result of the harmonic analysis for the flutter computation is presented in Figure 8. The imaginary part of the dimensionless pressure fluctuations on the suction side of the moving blade is plotted over the relative chord length. The imaginary part can be interpreted as the energetically meaningful part of the pressure fluctuations. It is therefore a measure for excitation or damping of the moving blade. As can be seen, the overall agreement of the computational and experimental results is good. Especially, the strong destabilizing influence of the shock impulse at about 25% chord length is well predicted. Integration of the pressure fluctuations over the whole blade for this operating point results in a negative damping, meaning that the blade would be excited to vibrate by the flow.

5.3. Clocking investigations

Reinmöller *et al.* [21] investigated the effects of stator airfoil clocking on the performance of a 1-1/2 stage axial cold air turbine experimentally and computationally at the Institute for Jet Propulsion and Turbomachinery. Experiments have been carried out for 10 clocking positions in steps of angles of 1° thus ranging over one blade pitch.

Three-dimensional, unsteady, viscous computations have been performed with the flow solver PANTA for 5 clocking positions in steps of angles of 2° thus also covering one

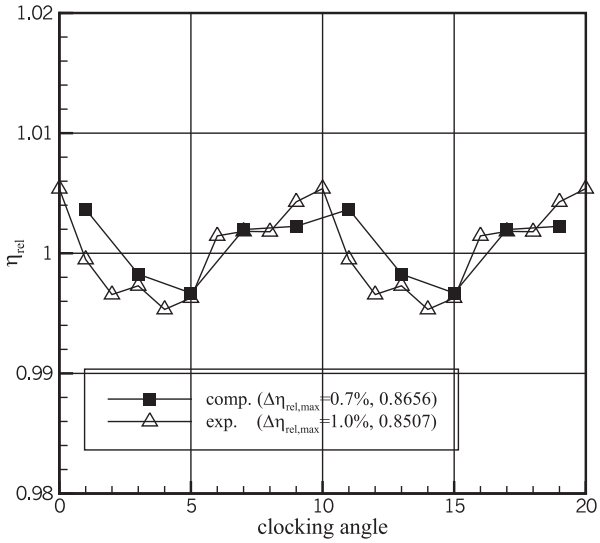

Figure 9. Computed and measured relative efficiencies

blade pitch. For the time-accurate, multistage calculations, which have been conducted on a single blade channel, phase-shifted periodic boundary conditions have been applied (Erdos *et al.* [22]). A partial surface concept at the sliding blade row interface takes into account the relative motion between the adjacent blade rows.

In Figure 9, the thermodynamic total-to-total efficiency calculated for the computed clocking positions is shown. Due to the fact that the precision of the temperature measurements strongly influences the calculated efficiency level, only the variations of η_{rel} (efficiency normalised by the average efficiency) are compared with experimental results at the midspan.

It can be seen that the qualitative variation of the relative efficiency versus the clocking angle is very similar to that observed in the measurements. The maximum can be found near a clocking angle of 0° and the minimum near a clocking angle of 5°. The maximum variation of efficiency is about $\Delta\eta_{rel,max} = 0.7\,\%$ for the numerical simulations ($\eta_{av} = 0.8656$) and about $\Delta\eta_{rel,max} = 1.0\,\%$ for the measurements ($\eta_{av} = 0.8507$).

Figure 10 shows the time-averaged entropy distributions at the midspan of the second stator for the highest (1°) and lowest (5°) efficiencies. In both contour plots the first stator wake with higher entropy values can clearly be detected at the same circumferential position. For the highest efficiency this region is located in the middle of the second stator passage, whereas for the lowest efficiency it can be found on the suction side of the second stator.

In view of the fact that the pitchwise flow angle in front of the second stator is influenced by the first stator wake, the airfoil loadings along the suction side of the second stator at the highest and lowest efficiencies are different. In Figure 11, it can be seen that the airfoil loading at the lowest efficiency (5°) is higher due to the reduced suction-sided incidence.

6. SUMMARY

A 3D Navier-Stokes package for the time-accurate computation of unsteady flows in turbomachines with emphasis on wide applicability, portability and efficiency is presented.

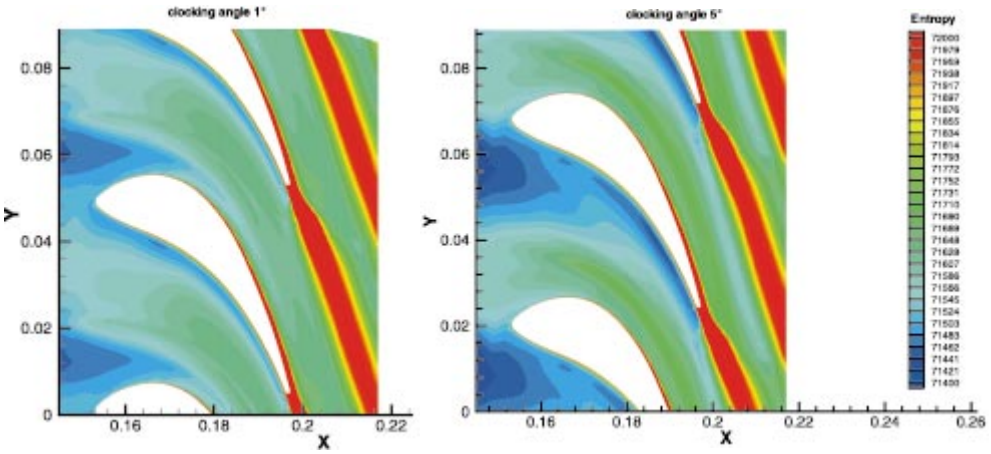

Figure 10. Time-averaged entropy distributions at midspan of the second stator for clocking angles of 1° (left) and 5° (right)

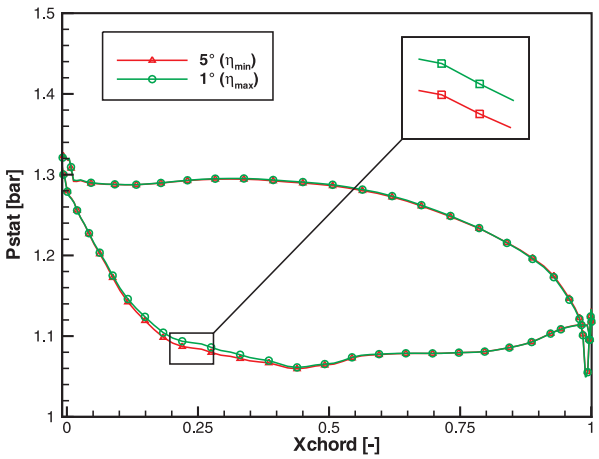

Figure 11. Static profile pressure of the second stator for clocking angles of 1° and 5°

The package consists of three components: the elliptic grid generator FRAME, the parallelised implicit Reynolds- and Favre-averaged Navier-Stokes solver PANTA and the post-processor TREAT especially designed for unsteady flow phenomena. Turbulent computations can be performed either with a Low-Reynolds-Number k-ε or k-ω turbulence model. Additionally, an algebraic transition model can be chosen from a variety of different models to enhance the accuracy of prediction for transitional flow phenomena.

The applicability of the package covers both rotor/stator interaction and blade flutter phenomena in multirow and multipassage 2D, Quasi3D and general 3D configurations in a wide range of flow velocities (subsonic, transonic) and has been demonstrated for various turbomachinery test cases within this paper.

Computations for an annular subsonic compressor cascade show that the prediction of the boundary layer development can be improved compared to fully turbulent computations when additional algebraic transition models are applied.

Flutter computations of a linear transonic compressor cascade at near stall conditions show a strong destabilizing influence of the shock impulse resulting in an overall negative aerodynamic damping of the oscillating blade.

Investigations of stator airfoil-clocking in a 1-1/2 stage axial cold air turbine show that clocking positions of maximum and minimum efficiency can be found in good agreement with experimental results.

References

[1] Benetschik H, Lohmann A, Lücke J R and Gallus H E 1996 *Inviscid and Viscous Analysis of Three-Dimensional Turbomachinery Flows Using an Implicit Upwind Algorithm* AIAA 96-2556

[2] Brouillet B, Benetschik H, Volmar T, Gallus H E and Niehuis R 1999 *3D Navier-Stokes Simulation of a Transonic Flutter Cascade Near Stall Conditions, International Gas Turbine Conference* in: Tamura T (ed.), Proc. of the International Gas Turbine Congress, Kobe, Japan, No 1, pp. 511–518

[3] Thompson J F 1984 *AIAA Journal* **22** (11) 1505

[4] Sorenson R L 1980 *A Computer Program to Generate Two-Dimensional Grids about Airfoils and Other Shapes by the Use of Poisson* NASA Technical Memorandum

[5] Chien K Y 1982 *AIAA Journal* **29** (2) 33

[6] Biswas D and Fukuyama Y 1993 *Calculation of Transitional Boundary Layers with an Improved Low-Reynolds-Number Version of the k-ε Turbulence Model* ASME 93-GT-73

[7] Wilcox D C 1993 *Turbulence Modeling for CFD* DCW

[8] Emmons H W 1951 *Journal of Aerospace Science* **18** (7) 490

[9] Roe P L 1981 *J. Comput. Phys.* **43** 357

[10] van Leer B 1979 *J. Comput. Phys.* **32** 101

[11] Chakravarthy S R 1988 *High Resolution Upwind Formulations for the Navier-Stokes Equations* Von Karman Institute for Fluid Dynamics – Lecture Series, No 5

[12] Müller M, Gallus H E and Niehuis R 2000 *A Study on Models to Simulate Boundary Layer Transition in Turbomachinery Flows* ASME 2000-GT-274

[13] Thermann H, Müller M and Niehuis R 2001 *Numerical Simulation of the Boundary Layer Transition in Turbomachinery Flows* ASME 2001-GT-475

[14] Schulz H D 1989 *Experimentelle Untersuchung der dreidimensionalen abgelösten Strömung in einem Axialverdichterringgitter* Dissertation RWTH Aachen

[15] Mayle R E 1991 *Journal of Turbomachinery* **113** 509

[16] Walker G J, Subroto P H and Platzer M F 1988 *Transition Modeling Effects on Viscous/Inviscid Interaction Analysis of Low Reynolds Number Airfoil Flows Involving Laminar Separation Bubbles* ASME 88-GT-32

[17] Sieger K, Schiele R, Kaufmann F, Wittig S and Rodi W 1995 *ERCOFTAC Bulletin* **24** 21

[18] Solomon W J, Walker G J and Gostelow J P 1996 *Journal of Turbomachinery* **118** (4) 744

[19] Poensgen C A and Gallus H E 1994 *Experimentelle Untersuchung an schwingenden Schaufeln* Abschlußbericht zum AG-Turbo Forschungsvorhaben 1.1.3.1, RWTH Aachen

[20] Ellenberger K and Gallus H E 1999 *Experimental Investigations of Stall Flutter in a Transonic Cascade* ASME 99-GT-409

[21] Reinmöller U, Stephan B, Schmidt S and Niehuis R 2001 *Clocking Effects in a 1.5 Stage Axial Turbine – Steady and Unsteady Experimental Investigations Supported by Numerical Simulations* ASME-GT-304

[22] Erdos J I, Alzner E and McNally W 1977 *AIAA Journal* **15** (11) 1559